A numerical approach for a system of transport equations in the field of radiotherapy

Teddy Pichard, Stéphane Brull, Bruno Dubroca

A numerical approach for a system of transport equations in the field of radiotherapy

Teddy Pichard, Stéphane Brull, Bruno Dubroca

September 6, 2017

Abstract

Numerical schemes for the systems of transport equations are commonly constrained by a stability condition of Courant-Friedrichs-Lewy (CFL) type. We consider here a system modeling the steady transport of photons and electrons in the field of radiotherapy, which leads to very stiff CFL conditions at the discrete level. We circumvent this issue by constructing an implicit scheme based on a relaxation approach.

The physics is modeled by an entropy-based moment system, namely the M_1 model. This model is non-linear, possesses potentially no hyperbolic operator. It is furthermore only valid under a condition called realizability, which corresponds to the positivity of an underlying kinetic distribution function.

The present numerical approach is applicable to non-linear systems which possess potentially no hyperbolic operator, and it preserves the realizability property. However the discrete equations are non-linear and we propose a numerical method to solve such non-linear systems.

Our approach is tested on academic and practical cases in 1D, 2D and 3D and it is shown to require significantly less computational power than reference methods.

Keyword: Implicit scheme ; Relaxation scheme ; M_1 model ; Radiotherapy dose computation

AMS: 35A35 ; 65M22 ; 35L65 ; 82C40

1 Introduction

This work aims to construct a numerical solver for systems of steady transport equations emerging in the field of radiotherapy. It is a follow-up to ([21, 5, 49]) and it analyses the numerical method used [46, 50, 48, 47, 14, 6, 45].

The motion of energetic particles in radiotherapy can be modeled by a system of coupled linear kinetic equations over the fluences of the particles, *i.e.* over distribution functions in a phase space composed of position $x \in \mathbb{R}^3$, energy $\epsilon \in \mathbb{R}^+$ and direction of flight $\Omega \in S^2$. Due to the high dimension of this phase space, solving directly such systems of equations, through either Monte Carlo methods ([32, 35, 15]) or discrete ordinates methods ([39]; see also [40] and references therein for a review on numerical approaches for dose computation) commonly requires much higher numerical powers than the standart available in medical centers.

As an alternative, an angular moment extraction technique is used. The obtained system is closed using an entropy minimization procedure leading to the so-called M_1 model. Such a closure was preferred as it is known to preserve the main features of the underlying kinetic model, and it models accurately beams of particles. This method was widely used for diverse applications in physics and biology *e.g.* in astrophysics ([16, 17, 27]), radiative transfer ([19, 51]), in fluid dynamics ([38, 41, 26]), in physics of semi-conductors ([29, 52]) or for chemotaxis modelling ([7]), and showed a considerable reduction of the numerical costs.

Numerical approaches for solving moment equations are typically restricted by a stability condition. Such a condition becomes very restrictive in the presence of low density media. This typically corresponds to require a step size (see [5, 49] or Section 3 below) proportional to the minimum density in the medium. This problem was first studied for application in radiotherapy in [5] and it was circumvented by the use of a clever change of variables. In [49], we proposed another approach based on a relaxation method (based on [43, 11, 1], see also recent work [18]) and on the method of characteristics. However, both those approaches are inappropriate to model the motion of photons. Indeed, those numerical schemes can be applied only if the considered system contains an hyperbolic operator, but the photon transport was shown to be ill-modeled by such a type of equations ([44]).

We propose here an implicit scheme based on the method of characteristics preserving the realizability property and efficient with large step size. However the obtained discretized equations are non-linear and an iterative

solver is constructed to solve such equations.

The paper is constructed as follows. In the next section, models of transport of photons and electrons are proposed, first at the kinetic level, then the angular moment extraction technique is described. A first numerical scheme is presented for 1D problems in Section 3, an iterative algorithm adapted to this scheme is proposed and tested on a practical test case. This numerical scheme is completed and adapted for multi-D problems in Section 4. Section 5 is devoted to conclusion.

2 Models of transport of photons and electrons

Photons and electrons are characterized their position $x \in \mathbb{R}^3$, their energy $\epsilon \in \mathbb{R}^+$ and their direction of flight $\Omega \in S^2$ on the unit sphere. The transported particles are assumed to interact only with atoms of the background medium. The influence of such interactions on the medium are neglected. In particular the composition of the medium is *a priori* given data.

2.1 A kinetic model

The motion of transported photons and electrons can be modeled by their fluences ψ_γ and ψ_e, *i.e.* densities in the (x, ϵ, Ω) space. They satisfy the following steady kinetic equations (see *e.g.* [23, 32])

$$\Omega.\nabla_x \psi_\gamma(x,\epsilon,\Omega) = \rho(x)\left[Q_{\gamma\to\gamma}(\psi_\gamma)(x,\epsilon,\Omega) + Q_{e\to\gamma}(\psi_e)(x,\epsilon,\Omega)\right], \quad (1a)$$

$$\Omega.\nabla_x \psi_e(x,\epsilon,\Omega) = \rho(x)\left[Q_{e\to e}(\psi_e)(x,\epsilon,\Omega) + Q_{\gamma\to e}(\psi_\gamma)(x,\epsilon,\Omega)\right], \quad (1b)$$

composed of time-independent free transport terms on the left-hand side and collisions operators on the right-hand side. The collision operator $Q_{\alpha\to\beta}$ models the variations of the fluence ψ_β due to the collisions involving incident particles α. The collision operator is chosen to be proportional to the relative density $\rho > 0$ compared to the density of water. As a first approximation, the influence of the composition of the medium on the collisions is neglected.

The considered collision operators are given by

$$\begin{aligned} Q_{\gamma\to\gamma}(\psi_\gamma) &= [G_{\gamma\to\gamma} - P_\gamma](\psi_\gamma), && \text{(2a)}\\ Q_{\gamma\to e}(\psi_\gamma) &= G_{\gamma\to e}(\psi_\gamma), && \text{(2b)}\\ Q_{e\to\gamma}(\psi_e) &= 0, && \text{(2c)}\\ Q_{e\to e}(\psi_e) &= \partial_\epsilon(S\psi_e) + [G_{e\to e} - P_e](\psi_e), && \text{(2d)} \end{aligned}$$

where the terms $G_{\alpha\to\beta}$ and P_β are linear Boltzmann gain and loss terms given by

$$\begin{aligned} G_{\alpha\to\beta}(\psi_\alpha)(\epsilon,x,\Omega) &= \int_\epsilon^{\epsilon_{\max}}\int_{S^2}\sigma_{\alpha\to\beta}(\epsilon',\epsilon,\Omega'.\Omega)\psi_\alpha(\epsilon',x,\Omega')d\epsilon' d\Omega', && \text{(2e)}\\ P_\beta(\psi_\beta)(\epsilon,x,\Omega) &= \sigma_{T,\beta}(\epsilon)\psi_\beta(\epsilon,x,\Omega). && \text{(2f)} \end{aligned}$$

The stopping power $S > 0$, the differential cross sections $\sigma_{\alpha\to\beta} \geq 0$ and the total cross sections $\sigma_{T,\beta} > 0$ are *a priori* given and characterize the collisions in a medium. Those collision operators (2) were chosen because they accurately model Compton, Møller, and elastic nuclear scattering (see *e.g.* [32, 23]) which are the predominant effects at the considered ranges of energy.

In medical physics, the function of interest is the energy deposited by the particles per mass unit, so-called dose. At the kinetic level, this dose D is simply given by

$$D(x) = \int_{\epsilon_{\min}}^{\epsilon_{\max}}\int_{S^2}(-\epsilon)\sum_{\alpha,\beta=\gamma,e} Q_{\alpha\to\beta}(\psi_\alpha)(x,\epsilon,\Omega)d\Omega d\epsilon. \tag{3}$$

2.2 A moment model

Solving numerically kinetic equations of the form (1-2) requires high computational power. Instead, the method of moments is often used as it requires lower computational power (see some comparisons *e.g.* in the previous work [49, 48, 46]).

In the following, the construction of the M_1 model associated to the kinetic model (1-2) is recalled.

The moments ψ^0, ψ^1 and ψ^2 of a fluence ψ are defined by

$$\psi^0(x,\epsilon) = \int_{S^2}\psi(x,\epsilon,\Omega)d\Omega, \qquad \psi^1(x,\epsilon) = \int_{S^2}\Omega\psi(x,\epsilon,\Omega)d\Omega, \tag{4}$$
$$\psi^2(x,\epsilon) = \int_{S^2}\Omega\otimes\Omega\psi(x,\epsilon,\Omega)d\Omega.$$

Equations on the moments are obtained by extracting moments of the kinetic equation (1). For moments up to order 1, it yields

$$\begin{aligned}
\nabla_x.\psi_\gamma^{i+1}(x,\epsilon) &= \rho(x)\left[Q^i_{\gamma\to\gamma}(\psi^i_\gamma)+Q^i_{e\to\gamma}(\psi^i_e)\right](x,\epsilon), &\text{(5a)}\\
\nabla_x.\psi_e^{i+1}(x,\epsilon) &= \rho(x)\left[Q^i_{e\to e}(\psi^i_e)+Q^i_{\gamma\to e}(\psi^i_\gamma)\right](x,\epsilon), &\text{(5b)}
\end{aligned}$$

for $i=0,1$, and the moments of the collision operators of order i are

$$\begin{aligned}
Q^i_{\gamma\to\gamma}(\psi_\gamma) &= \left[G^i_{\gamma\to\gamma}-P^i_\gamma\right](\psi^i_\gamma), &\text{(5c)}\\
Q^i_{\gamma\to e}(\psi_\gamma) &= G^i_{\gamma\to e}(\psi^i_\gamma), &\text{(5d)}\\
Q^i_{e\to\gamma}(\psi_e) &= 0, &\text{(5e)}\\
Q^i_{e\to e}(\psi_e) &= \partial_\epsilon(S\psi^i_e)+\left[G^i_{e\to e}-P^i_e\right](\psi^i_e), &\text{(5f)}
\end{aligned}$$

where the terms $G^i_{\alpha\to\beta}$ and P^i_β read

$$\begin{aligned}
G^i_{\alpha\to\beta}(\psi^i_\alpha)(\epsilon,x) &= \int_\epsilon^{\epsilon_{\max}}\sigma^i_{\alpha\to\beta}(\epsilon',\epsilon)\psi^i_\alpha(\epsilon',x)d\epsilon', &\text{(5g)}\\
P^i_\beta(\psi^i_\beta)(\epsilon,x) &= \sigma_{T,\beta}(\epsilon)\psi^i_\beta(\epsilon,x), &\text{(5h)}\\
\sigma^i_{\alpha\to\beta}(\epsilon',\epsilon) &= 2\pi\int_{-1}^{+1}\mu^i\sigma_{\alpha\to\beta}(\epsilon',\epsilon,\mu)d\mu. &\text{(5i)}
\end{aligned}$$

Remark 1. Due to the integrals in the collision operators (5g), when working at energy ϵ, one needs the knowledge of the fluence of the particles at all energy $\epsilon' \in [\epsilon, \epsilon_{max}]$. In practice, the equations are solved from a maximum energy ϵ_{max} to a minimum energy ϵ_{min}.

The system (5) is underdetermined. To solve it, the system is completed with one more relation, so-called M_1 closure ([42, 38]), expressing ψ^2_α as a function of ψ^0_α and ψ^1_α for $\alpha=\gamma,e$. This closure consists in reconstructing the unique function ([8, 9, 10, 38, 54, 31, 30]) of the form

$$\psi_{M_1}(\Omega)=\exp(\boldsymbol{\lambda}.\mathbf{m}(\Omega)), \qquad \mathbf{m}(\Omega)=(1,\ \Omega_1,\ \Omega_2,\ \Omega_3), \tag{6}$$

with $\boldsymbol{\lambda}\in\mathbb{R}^4$ such that

$$\int_{S^2}\psi_{M_1}(\Omega)d\Omega=\psi^0, \qquad \int_{S^2}\Omega\psi_{M_1}(\Omega)d\Omega=\psi^1, \tag{7}$$

then express the last moment as

$$\psi^2=\int_{S^2}\Omega\otimes\Omega\psi_{M_1}(\Omega)d\Omega. \tag{8}$$

Definition 1. The M_1 closure is defined only if there exists a function of the form (6) satisfying (7). Such a function was shown to exists if and only if ([34])

$$(\psi^0, \psi^1) \in \mathcal{R} \quad = \quad \left\{(f^0, f^1) \in \mathbb{R}^4, \quad \text{s.t.} \quad |f^1| < f^0\right\}. \tag{9}$$

This condition needs to be kept in mind when constructing numerical schemes. In particular, in the next section we will use the following remark.

Remark 2. The realizability domain is a convex cone.

Since the differential cross sections $\sigma_{\alpha\to\beta}$ are also positive, their moments need to satisfy the following realizability condition ([34])

$$|\sigma^1_{\alpha\to\beta}| \leq \sigma^0_{\alpha\to\beta}. \tag{10}$$

3 A discretization for 1D problems

We aim to construct a solver for the moment system (5).

For the sake of simplicity, the numerical approach is described for problems in one spatial dimension. The results are generalized to multidimensional problems in the next section.

In the first subsection, the main problem with the discretization of (5) is presented. A first numerical method is proposed in the remaining subsections.

3.1 The fast characteristics problem in 1D

First the problem (5) is rewritten, then the main difficulty emerging when discretizing the rewritten equations is presented.

3.1.1 Problem settings

In 1D, the system (5) can be rewritten under the vectorial form

$$\partial_x \mathbf{F}(\boldsymbol{\psi})(x,\epsilon) \quad = \quad \rho(x)\mathbf{Q}(\boldsymbol{\psi})(x,\epsilon), \tag{11a}$$

where the unknown is $\boldsymbol{\psi} = \left(\boldsymbol{\psi}_\gamma,\ \boldsymbol{\psi}_e\right)$, and $\boldsymbol{\psi}_\alpha = (\psi^0_\alpha,\ \psi^1_\alpha)$ are the moments of the fluence of particles $\alpha = \gamma, e$. The fluxes $\mathbf{F}(\boldsymbol{\psi})$ and the collision operator

$\mathbf{Q}(\boldsymbol{\psi})$ are defined over $\mathcal{R}^2$ by

$$\begin{aligned} \mathbf{F}(\boldsymbol{\psi}) &= \left(\mathbf{F}_{M_1}(\boldsymbol{\psi}_\gamma),\ \mathbf{F}_{M_1}(\boldsymbol{\psi}_e)\right), & \text{(11b)} \\ \mathbf{Q}(\boldsymbol{\psi}) &= \left(\mathbf{Q}_{\gamma\to\gamma}(\boldsymbol{\psi}_\gamma)+\mathbf{Q}_{e\to\gamma}(\boldsymbol{\psi}_e),\ \mathbf{Q}_{e\to e}(\boldsymbol{\psi}_e)+\mathbf{Q}_{\gamma\to e}(\boldsymbol{\psi}_\gamma)\right), & \text{(11c)} \end{aligned}$$

and are composed of the moments of the kinetic flux and collision operator according to

$$\begin{aligned} \mathbf{F}_{M_1}(\boldsymbol{\psi}_\alpha) &= (\psi^1_\alpha,\ \psi^2_\alpha), & \text{(11d)} \\ \mathbf{Q}_{\alpha\to\beta}(\boldsymbol{\psi}_\alpha) &= \left(Q^0_{\alpha\to\beta}(\psi^0_\alpha),\ Q^1_{\alpha\to\beta}(\psi^1_\alpha)\right), & \text{(11e)} \end{aligned}$$

where ψ^2_α is given by the closure relation (8). Before describing the numerical approaches, the following notations are introduced.

Notation 1. The superscript n refers to the discretization in energy ϵ and the subscript l to the discretization in the x variable. In the next section, the subscript m will refer to the discretization in the second space variable y.

According to Remark 1, the energy grid is such that $\epsilon^n > \epsilon^{n+1}$.

3.1.2 Position of the problem

Standart methods to solve (11a) in the field of radiotherapy present stiff terms which make such methods very time-consuming for practical applications. This stiffness arises in weakly collisional media, *e.g.* when the background medium has a low density ρ, in which the effect of the collisions becomes negligible. This problem was illustrated in [5, 49] through a 1D electron transport equation of the form

$$\partial_x \mathbf{F}_{M_1}(\boldsymbol{\psi}_e) = \rho\left[\partial_\epsilon(S\boldsymbol{\psi}_e) + A\boldsymbol{\psi}_e\right], \qquad A = \begin{pmatrix} 0 & 0 \\ 0 & T \end{pmatrix}, \tag{12}$$

with $T \in \mathbb{R}^+$ by using an HLL-like ([28]) scheme defined by

$$\frac{\mathbf{F}^n_{e,l+\frac{1}{2}} - \mathbf{F}^n_{e,l-\frac{1}{2}}}{\Delta x} - \rho_l \frac{S^n\boldsymbol{\psi}^n_{e,l} - S^{n+1}\boldsymbol{\psi}^{n+1}_{e,l}}{\Delta\epsilon^n} = \rho_l A^n \boldsymbol{\psi}^n_{e,l}, \tag{13a}$$

with a numerical flux given by

$$\mathbf{F}^n_{e,l+\frac{1}{2}} = \frac{1}{2}\left[\mathbf{F}_{M_1}(\boldsymbol{\psi}^n_{e,l+1}) + \mathbf{F}_{M_1}(\boldsymbol{\psi}^n_{e,l}) + (\boldsymbol{\psi}^n_{e,l+1} - \boldsymbol{\psi}^n_{e,l})\right]. \tag{13b}$$

Such a scheme was shown to be consistent with (12), however it is only stable under the following Courant-Friedrichs-Lewy (CFL) condition

$$\Delta\epsilon^n \leq S^n \Delta x \min_l(\rho_l). \tag{14}$$

The condition (14) turns very restrictive when considering low collisional media, here when ρ is small. In such a case, one requires a very large number of energy steps and therefore considerably long computational times are necessary.

A first solution to this problem was proposed in [5] by the use of a change of variable. An alternative was proposed in [49] through a method of characteristic applied on a relaxed system for (12). However, both methods can only be used when the considered equation possesses an hyperbolic operator, and are therefore not applicable to the coupled photons-electrons transport equations (5).

The present discretization of the system (11) is presented in three parts.

- **Step 1** (Subsection 3.2): the advection operator is discretized, this corresponds to the discretization over the position variable x.
- **Step 2** (Subsection 3.3): the collision operator is discretized, this corresponds to the discretization over the energy variable ϵ.
- **Step 3** (Subsection 3.4): both discretizations are gathered to construct a numerical scheme and an iterative algorithm is proposed to solve the obtained discrete equations.

3.2 Discretization of the advection operator

In the spirit of [49], we propose a numerical scheme for (5) based on the relaxation method developed in [43, 11, 12, 1]. The principle of the relaxation method is first recalled.

Instead of studying directly (5), one studies the following relaxed equations

$$c^- \partial_x \mathbf{f}_\tau^- - \rho \mathbf{Q}(\mathbf{f}_\tau^-) = \frac{\mathbf{M}^- - \mathbf{f}_\tau^-}{\tau}, \tag{15a}$$

$$c^+ \partial_x \mathbf{f}_\tau^+ - \rho \mathbf{Q}(\mathbf{f}_\tau^+) = \frac{\mathbf{M}^+ - \mathbf{f}_\tau^+}{\tau}, \tag{15b}$$

where $\mathbf{f}_\tau^\pm$ are the unknowns relaxing toward the equilibrium represented by the Maxwellians $\mathbf{M}^\pm(\boldsymbol{\psi}) \in \mathcal{R}^2$, and τ is a relaxation parameter. The relaxation velocities $c^\pm(\boldsymbol{\psi}) \in \mathbb{R}$ are chosen such that they bound the physical velocities. This leads to the following stability requirement

$$Sp\left(\mathbf{F}'(\boldsymbol{\psi})\right) \quad \subset \quad [c^-,\ c^+]. \tag{16a}$$

The Maxwellians $\mathbf{M}^\pm(\boldsymbol{\psi}) \in \mathcal{R}^2$ are chosen to relate to the original system through the following consistency formulae

$$\mathbf{M}^+ + \mathbf{M}^- = \boldsymbol{\psi}, \qquad c^+\mathbf{M}^+ + c^-\mathbf{M}^- = \mathbf{F}(\boldsymbol{\psi}). \tag{16b}$$

Formally, at the limit $\tau \to 0$ in (15), one obtains $\mathbf{f}_0^\pm = \mathbf{M}^\pm$. Then replacing $\mathbf{f}^\pm$ by $\mathbf{M}^\pm$ and summing the two equations (15) yields (11). Therefore, one retreives the solution of the original equation (11) in the limit case $\tau \to 0$ as

$$\boldsymbol{\psi} = \lim_{\tau \to 0} \left(\mathbf{f}_\tau^+ + \mathbf{f}_\tau^-\right). \tag{17}$$

We refer to [43, 11, 1, 12, 2] for a proper analysis of this asymptotic limit.

For the sake of simplicity, in the 1D case, we use the following classical result (see *e.g.* [13, 4, 49]), to chose relaxation parameters.

Lemma 1. *The eigenvalues of the Jacobian $\mathbf{F}'_{M_1}(\psi)$ of the M_1 fluxes are bounded by 1 for all $\boldsymbol{\psi} \in \mathcal{R}$, that is*

$$\forall \boldsymbol{\psi} \in \mathcal{R}, \quad Sp(\mathbf{F}'_{M_1}(\boldsymbol{\psi})) \subset]-1, 1[.$$

Furthermore, for all realizable moments $\boldsymbol{\psi} \in \mathcal{R}$, one has

$$\boldsymbol{\psi} \pm \mathbf{F}_{M_1}(\boldsymbol{\psi}) \in \mathcal{R}.$$

Thus, in 1D, we will use the following parameters

$$c^+ = 1 = -c^-, \qquad \mathbf{M}^\pm = \frac{\boldsymbol{\psi} \pm \mathbf{F}(\boldsymbol{\psi})}{2} \in \mathcal{R}^2, \tag{18a}$$

$$\pm \partial_x \mathbf{f}_\tau^\pm - \rho \mathbf{Q}(\mathbf{f}_\tau^\pm) = \frac{\mathbf{M}^\pm - \mathbf{f}_\tau^\pm}{\tau}, \tag{18b}$$

which satisfy the requirements (16).

Then we use upwind fluxes on (18b) leading to the scheme

$$\frac{\mathbf{f}_{\tau,l}^{\pm,n} - \mathbf{f}_{\tau,l\mp1}^{\pm,n}}{\Delta x} - \rho \mathbf{Q}(\mathbf{f}_{\tau,l}^{\pm,n}) = \frac{\mathbf{M}^\pm - \mathbf{f}_{\tau,l}^{\pm,n}}{\tau}. \tag{19}$$

Then summing these equations over $\pm$ and having $\tau \to 0$ leads to define the following scheme over $\boldsymbol{\psi}$

$$\frac{\mathbf{F}^n_{l+\frac{1}{2}} - \mathbf{F}^n_{l-\frac{1}{2}}}{\Delta x} - [\rho \mathbf{Q}(\boldsymbol{\psi})]^n_l = 0, \tag{20a}$$

$$\mathbf{F}^n_{l+\frac{1}{2}} = \frac{1}{2}\left[\mathbf{F}(\boldsymbol{\psi}^n_{l+1}) + \mathbf{F}(\boldsymbol{\psi}^n_l) - (\boldsymbol{\psi}^n_{l+1} - \boldsymbol{\psi}^n_l)\right]. \tag{20b}$$

The term $[\rho \mathbf{Q}(\boldsymbol{\psi})]^n_l$ will be defined in the next subsection.

Remark 3. Since the collision operator $\mathbf{Q}$ is linear, one should retreive

$$\mathbf{Q}(\boldsymbol{\psi})^n_l = \mathbf{Q}(\mathbf{M}^- + \mathbf{M}^+)^n_l = \mathbf{Q}(\mathbf{M}^-)^n_l + \mathbf{Q}(\mathbf{M}^+)^n_l.$$

3.3 Discretization of the collision operator

The collision terms are simply discretized with a quadrature rule for the integrals in ϵ at the points ϵ^n and an implicit Euler discretization for the term $\partial_\epsilon(S\boldsymbol{\psi}_e)$. This reads

$$[\rho \mathbf{Q}(\boldsymbol{\psi})]^n_l = \rho_l \mathbf{Q}(\boldsymbol{\psi})^n_l, \tag{21a}$$

$$\mathbf{Q}(\boldsymbol{\psi})^n_l = \big(\mathbf{Q}_{\gamma\to\gamma}(\boldsymbol{\psi}_\gamma)^n_l + \mathbf{Q}_{e\to\gamma}(\boldsymbol{\psi}_e)^n_l, \mathbf{Q}_{e\to e}(\boldsymbol{\psi}_e)^n_l + \mathbf{Q}_{\gamma\to\gamma}(\boldsymbol{\psi}_\gamma)^n_l\big), \tag{21b}$$

$$\mathbf{Q}_{\alpha\to\beta}(\boldsymbol{\psi}_\alpha)^n_l = \big(Q^0_{\alpha\to\beta}(\psi^0_\alpha)^n_l,\ Q^1_{\alpha\to\beta}(\psi^1_\alpha)^n_l\big), \tag{21c}$$

where each discrete collision operators is, for $i = 0, 1$

$$Q^i_{\gamma\to\gamma}(\psi^i_\gamma)^n_l = \sum_{n'=1}^{n} \sigma^{i,n',n}_{\gamma\to\gamma} \psi^{i,n'}_{\gamma,l} \Delta\epsilon^{n'} - \sigma^n_{T,\gamma} \psi^{i,n}_{\gamma,l}, \tag{21d}$$

$$Q^i_{\gamma\to e}(\psi^i_\gamma)^n_l = \sum_{n'=1}^{n} \sigma^{i,n',n}_{\gamma\to e} \psi^{i,n'}_{\gamma,l} \Delta\epsilon^{n'}, \qquad Q^i_{e\to\gamma}(\psi^i_e)^n_l = 0, \tag{21e}$$

$$Q^i_{e\to e}(\psi^i_e)^n_l = \frac{S^{n-1}\psi^{i,n-1}_{e,l} - S^n \psi^{i,n}_{e,l}}{\Delta\epsilon^n} + \sum_{n'=1}^{n} \sigma^{i,n',n}_{e\to e} \psi^{i,n'}_{e,l} \Delta\epsilon^{n'} - \sigma^n_{T,e} \psi^{i,n}_{e,l}. \tag{21f}$$

Remark 4.

- We chose this particular discretization because it leads to an implicit scheme, in the sense that the fluxes $\mathbf{F}^n_{l+\frac{1}{2}}$ are evaluated at the latest energy step ϵ^n. In practice, the obtained scheme is efficient even without imposing a restriction on the step size $\Delta\epsilon^n$, which circumvents the problem presented in Subsection 3.1.

- All the discretizations presented here are of order one in Δx and in $\Delta\epsilon^n$, so the scheme (20-21) is consistent with the continuous equation (11a).

- In order to use the present scheme, one needs to compute $\boldsymbol{\psi}_l^n$ for all l. Here, this implies solving the non-linear equation (20-21) over the vector $(\boldsymbol{\psi}_l^n)_{l=1,\dots,l_{\max}} \in (\mathcal{R}^2)^{l_{\max}}$.

3.4 An iterative solver for the 1D scheme

Writing together the discretization of the 1D advection and the collision term with the relaxation parameters (18) yields the following numerical scheme

$$-\mathbf{L}(\boldsymbol{\psi}_{l-1}^n) + \mathbf{D}(\boldsymbol{\psi}_l^n) - \mathbf{U}(\boldsymbol{\psi}_{l+1}^n) = \rho_l \mathbf{R}_l^n, \tag{22a}$$

where the operators $\mathbf{L}$ and $\mathbf{U}$ are non-linear and $\mathbf{D}$ is linear and invertible. They are given by

$$\mathbf{L}(\boldsymbol{\psi}_{l-1}^n) = \frac{\boldsymbol{\psi}_{l-1}^n + \mathbf{F}(\boldsymbol{\psi}_{l-1}^n)}{2\Delta x}, \qquad \mathbf{U}(\boldsymbol{\psi}_{l+1}^n) = \frac{\boldsymbol{\psi}_{l+1}^n - \mathbf{F}(\boldsymbol{\psi}_{l+1}^n)}{2\Delta x}, \tag{22b}$$

$$\mathbf{D}(\boldsymbol{\psi}_l^n) = \left(\frac{Id}{\Delta x} + \rho_l A^n\right)\boldsymbol{\psi}_l^n, \tag{22c}$$

and A^n and $\mathbf{R}_l^n$ are given by

$$A^n\boldsymbol{\psi}_l^n = \left(B_0^n\boldsymbol{\psi}_l^n, \quad B_1^n\boldsymbol{\psi}_l^n, \quad D_0^n\boldsymbol{\psi}_l^n, \quad D_1^n\boldsymbol{\psi}_l^n\right), \tag{22d}$$

$$\mathbf{R}_l^n = (C_0^n, \quad C_1^n, \quad E_0^n, \quad E_1^n) + BC_l^n, \tag{22e}$$

with, for $i = 0, 1$,

$$B_i^n \boldsymbol{\psi}_l^n = (\sigma_{T,\gamma}^n - \sigma_{\gamma\to\gamma}^{i,n,n}\Delta\epsilon^n)\psi_{\gamma,l}^{i,n}, \qquad C_i^n = \sum_{n'=1}^{n-1} \sigma_{\gamma\to\gamma}^{i,n',n}\psi_{\gamma,l}^{i,n'}\Delta\epsilon^{n'}, \tag{22f}$$

$$D_i^n \boldsymbol{\psi}_l^n = \left(\frac{S^n}{\Delta\epsilon^n} + \sigma_{T,e}^n - \sigma_{e\to e}^{i,n,n}\Delta\epsilon^n\right)\psi_{e,l}^{i,n} - \sigma_{\gamma\to e}^{i,n,n}\psi_{\gamma,l}^{i,n}\Delta\epsilon^n, \tag{22g}$$

$$E_i^n = \frac{S^{n-1}}{\Delta\epsilon^n}\psi_{e,l}^{i,n-1} + \sum_{n'=1}^{n-1}\left(\sigma_{\gamma\to\gamma}^{i,n',n}\psi_{\gamma,l}^{i,n'} + \sigma_{e\to e}^{i,n',n}\psi_{e,l}^{i,n'}\right)\Delta\epsilon^{n'}. \tag{22h}$$

Defining properly boundary conditions for moment models based on the underlying kinetic ones remains an open problem (see *e.g.* [36, 53, 25] for linear moment equations). For the sake of simplicity, we use here discrete boundary conditions defined as a source term in (22e) with

$$BC_l^n = \boldsymbol{\psi}_0^n \delta_{1,l} + \boldsymbol{\psi}_{l_{\max}+1}^n \delta_{l_{\max},l},$$

with given $\boldsymbol{\psi}_0^n \in \mathcal{R}^2$ and $\boldsymbol{\psi}_{l_{\max}+1}^n \in \mathcal{R}^2$.

In order to use this scheme, one needs to solve (22) which is a non-linear equation on the vector $(\boldsymbol{\psi}^n)_{l=1,\dots,l_{\max}}$. For this purpose, we propose an iterative solver inspired of [20], which was tested in [48, 47, 50, 6, 45].

Algorithm 1. *Initialization:* Set $\boldsymbol{\psi}_l^{n,(0)} = \boldsymbol{\psi}_l^{n-1}$ for all l.
Iteration: Compute iteratively

$$\boldsymbol{\psi}_l^{n,(k+1)} = \mathbf{D}^{-1}\left(\mathbf{L}(\boldsymbol{\psi}_{l-1}^{n,(k)}) + \mathbf{U}(\boldsymbol{\psi}_{l+1}^{n,(k)}) + \rho_l \mathbf{R}_l^n\right), \tag{23}$$

until convergence.

Proposition 1. *Suppose that $\mathbf{R}_l^n \in \mathcal{R}^2$ is realizable for all l, and that*

$$\min_l \rho_l \min Sp(A^n)\Delta x > \sup_{\boldsymbol{\psi}\in\mathcal{R}^2}\left(\frac{(\max - \min)}{2}\left[Sp(F'(\boldsymbol{\psi}))\right]\right), \tag{24}$$

then there exists a unique solution $(\boldsymbol{\psi}^n)_{l=1,\dots,l_{\max}} \in (\mathcal{R}^2)^{l_{\max}}$ satisfying (22) for all l.
Moreover, Algorithm 1 converges to this solution.

Proof. Define the operator J over $\boldsymbol{\psi} \in (\mathcal{R}^2)^{l_{\max}}$ by

$$\boldsymbol{\psi}^{n,(k+1)} \;=\; J(\boldsymbol{\psi}^{n,(k)}),$$

where the l-th component $J(\boldsymbol{\psi}^{n,(k+1)})_l$ is given by (23), that is

$$\begin{aligned} J(\boldsymbol{\psi}^{n,(k+1)})_l \;=\; & \left(\frac{Id}{\Delta x} + \rho_l A^n\right)^{-1} \Bigg[\rho_l \mathbf{R}_l^n \\ & + \frac{\boldsymbol{\psi}_{l+1}^{n,(k)} - \mathbf{F}(\boldsymbol{\psi}_{l+1}^{n,(k)})}{2\Delta x} + \frac{\boldsymbol{\psi}_{l-1}^{n,(k)} + \mathbf{F}(\boldsymbol{\psi}_{l-1}^{n,(k)})}{2\Delta x}\Bigg]. \end{aligned} \tag{25}$$

First, we verify that J preserves the realizability from one step to another.

Let us suppose $\boldsymbol{\psi}^{n,(k)} \in (\mathcal{R}^2)^{l_{max}}$. Then $\boldsymbol{\psi}_{l+1}^{n,(k)} - \mathbf{F}(\boldsymbol{\psi}_{l+1}^{n,(k)}) \in \mathcal{R}^2$ and $\boldsymbol{\psi}_{l-1}^{n,(k)} + \mathbf{F}(\boldsymbol{\psi}_{l-1}^{n,(k)}) \in \mathcal{R}^2$ are realizable according to the second part of Lemma 1. Thus the term between square brackets in (25) is realizable accordig to remark 2.

Now, we need to prove that the operator $(\frac{Id}{\Delta x} + \rho_l A^n)^{-1}$ preserves the realizability property. Using its definition (22), the matrix A^n can be rewritten

$$A^n = \begin{pmatrix} a_0 & 0 & 0 & 0 \\ 0 & a_1 & 0 & 0 \\ b_0 & 0 & c_0 & 0 \\ 0 & b_1 & 0 & c_1 \end{pmatrix}, \quad \left(\frac{Id}{\Delta x} + \rho_l A^n\right)^{-1} = \begin{pmatrix} \alpha_0 & 0 & 0 & 0 \\ 0 & \alpha_1 & 0 & 0 \\ \beta_0 & 0 & \gamma_0 & 0 \\ 0 & \beta_1 & 0 & \gamma_1 \end{pmatrix}$$

where

$$\begin{aligned} a_i &= \sigma_{T,\gamma}^n - \sigma_{\gamma\to\gamma}^{i,n,n}\Delta\epsilon^n, & \alpha_i &= \frac{1}{\frac{1}{\Delta x} + \rho_l a_i}, \\ b_i &= -\sigma_{\gamma\to e}^{i,n,n}\Delta\epsilon^n, & \beta_i &= -\frac{b_i}{(\frac{1}{\Delta x} + \rho_l a_i)(\frac{1}{\Delta x} + \rho_l c_i)}, \\ c_i &= \frac{S^n}{\Delta\epsilon^n} + \sigma_{T,e}^n - \sigma_{e\to e}^{i,n,n}\Delta\epsilon^n, & \gamma_i &= \frac{1}{\frac{1}{\Delta x} + \rho_l c_i}. \end{aligned}$$

Using (10) leads to

$$a_0 \le a_1, \qquad c_0 \le c_1 \quad \text{and} \quad -b_0 \ge -b_1.$$

Then using the criteria (9), one verifies that the operator $\left(\frac{Id}{\Delta x} + \rho_l A^n\right)^{-1}$ preserves the realizability, so J is an operator from $(\mathcal{R}^2)^{l_{\max}}$ into itself.

Now, in order to prove that Algorithm 1 converges, we prove that J is a contraction. Derivating $J(\boldsymbol{\psi})$ according to $\boldsymbol{\psi}$ reads

$$d_{\boldsymbol{\psi}}J(\boldsymbol{\psi})_l.h = \left(\frac{Id}{\Delta x}+\rho_l A^n\right)^{-1}\left[\left(\frac{Id-\mathbf{F}'(\boldsymbol{\psi}_{l+1})}{2\Delta x}\right).h_{l+1} + \left(\frac{Id+\mathbf{F}'(\boldsymbol{\psi}_{l-1})}{2\Delta x}\right).h_{l-1}\right], \quad (26)$$

so $d_{\boldsymbol{\psi}}J(\boldsymbol{\psi})$ is a block matrix with non-zero blocks on the super- and sub-diagonal.

Using a Gershgörin theorem for block matrices ([55]) provides

$$Sp\left(d_{\boldsymbol{\psi}}J(\boldsymbol{\psi})\right) \subset [-r, r],$$

with a spectral radius satisfying

$$r \leq \max_l \frac{|||Id-F'(\boldsymbol{\psi_l})||| + |||Id+F'(\boldsymbol{\psi_l})|||}{2\min Sp(Id+\rho_l A^n\Delta x)}.$$

Using Lemma 1 and the fact that A^n is positive definite, one finds

$$r \leq \max_l \frac{1+\frac{(\max-\min)}{2}Sp(F'(\boldsymbol{\psi_l}))}{1+\rho_l \min Sp(A^n)\Delta x}, \quad (27)$$

thus $r < 1$ under condition (24), so J is a contraction and Algorithm 1 converges to the unique fixed point of J. □

Remark 5.

- The requirement (24) corresponds to a CFL-like condition. This condition was added here to prove at the theoretical level the convergence of the algorithm. Though the bound (27) used in the proof is *a priori* not optimal. And we have not yet found any theoretical nor experimental test case violating (24) that lead to a non-converging sequence $(\boldsymbol{\psi}^{n,(k)})_{k=1,\ldots,\infty}$, even with very low collisional media (for small ρ_l). In the test cases below, Δx and $\Delta\epsilon^n$ do not necessarily respect this condition and we always verify experimentally the convergence of Algorithm 1. We refer *e.g.* to [22, 56, 3, 33] and references therein for more complete study on convergence for such a type of algorithms.

- The iterative method proposed in Algorithm 1 can be interpreted as a Jacobi method with non-linear extradiagonal term. Similarily, Gauss-Seidel and successive over-relaxation (SOR) methods for this non-linear

problem can also be implemented. For example, the non-linear Gauss-Seidel type method consists in solving alternatively

$$\boldsymbol{\psi}_l^{n,(k+1)} = \mathbf{D}^{-1}\left(\mathbf{L}(\boldsymbol{\psi}_{l-1}^{n,(k+1)}) + \mathbf{U}(\boldsymbol{\psi}_{l+1}^{n,(k)}) + \rho_l \mathbf{R}_l^n\right), \tag{28a}$$

$$\boldsymbol{\psi}_l^{n,(k+1)} = \mathbf{D}^{-1}\left(\mathbf{L}(\boldsymbol{\psi}_{l-1}^{n,(k)}) + \mathbf{U}(\boldsymbol{\psi}_{l+1}^{n,(k+1)}) + \rho_l \mathbf{R}_l^n\right), \tag{28b}$$

in Algorithm 1 instead of (23). One can prove similarily that such algorithms are convergent.

- The convergence rate of Algorithm 1 depends on the eigenvalues of $d_{\boldsymbol{\psi}} J(\boldsymbol{\psi})$. In the computations (27), the worst possible convergence rate corresponds to the case where $(\max - \min)(Sp(F'(\boldsymbol{\psi_l})))$ has the highest value. Such highest value is obtained in the limit case of a purely anisotropic distribution (see *e.g.* computations in [4]) modeled by a fluence

  $$\psi(\Omega) = K\delta_{\Omega_1 - 1}.$$

  Thus Algorithm 1 is slower if the expected solution of (1) possesses purely anisotropic region.

3.5 Numerical experiments

This subsection is devoted to study experimentally the convergence of the present method. Especially, two convergence rates are studied:

- The convergence according to the number $k_{\max}$ of iterations in Algorithm 1.
- The convergence according to the cells size $\Delta\epsilon^n$ and Δx of the numerical scheme (22).

Those two convergence rates are observed through a numerical test case proposed in [48, 47].

A beam of electrons is imposed on the boundary of a 1D domain $Z = [0\ \text{cm}, 6\ \text{cm}]$ uniformly composed of water (*i.e.* $\rho = 1$). The beam is modeled by a boundary condition which corresponds to extracting the moments of

distributions of the form

$$\text{for} \quad \Omega_1 > 0, \quad \psi_e(0 \text{ cm}, \epsilon, \Omega) = K \exp\left(-c_e(\epsilon_0 - \epsilon)^2\right) \exp\left(-c_o(1-\Omega_1)^2\right), \quad \psi_\gamma(0 \text{ cm}, \epsilon, \Omega) = 0, \tag{29a}$$

$$\text{for} \quad \Omega_1 < 0, \quad \psi_e(6 \text{ cm}, \epsilon, \Omega) = \delta, \quad \psi_\gamma(6 \text{ cm}, \epsilon, \Omega) = 0, \tag{29b}$$

where the constants $c_e = 200$, $\epsilon_0 = 10$ MeV and $c_o = 1000$. The constants $K = 10^{10}$ and $\delta = 10^{-15}$ are chosen respectively arbitrarily high and low in order to avoid numerical divisions by zero. And the initial condition is fixed at $\psi_\alpha(11 \text{ MeV}, x, \Omega) = 0$ for $\alpha = \gamma$, e.

Remark that the equations of system (1) are decoupled. As we impose no source of photons, and due to the considered physiscs, no photons are created in the system. Thus the solution of (1a) is simply $\psi_\gamma = 0$, and the discretization (22) can be simplified when considering beams of electrons only. This is no longer true when considering more complex physics, *e.g.* when taking into account Bremsstrahlung effect [40, 37].

The mesh is composed of 600 cells in x uniformly distributed. The step size $\Delta\epsilon^n$ and the grid in ϵ are chosen such that

$$\Delta\epsilon^n = 5S^n\Delta x. \tag{30}$$

This corresponds approximately to fixing

$$\min Sp(A^n)\Delta x = 5.$$

With such a gridsize, we aim to avoid to have numerical diffusion effects depending $\Delta\epsilon^n$.

As an indication, the converged dose normalized by its maximum value, computed with Algorithm 1 is represented on Fig. 1. For more examples with different applications in medical physics, we refer *e.g.* to [6, 45, 50, 48].

3.5.1 Convergence results of the iterative algorithm

The iterative method of Algorithm 1 requires a criterium to stop.

A first naive criterium consists in fixing the number of iterations k_{max}. This is not optimal, neither in terms of precision nor in terms of computational costs. At each energy step, the desired solution follows (22). Then one

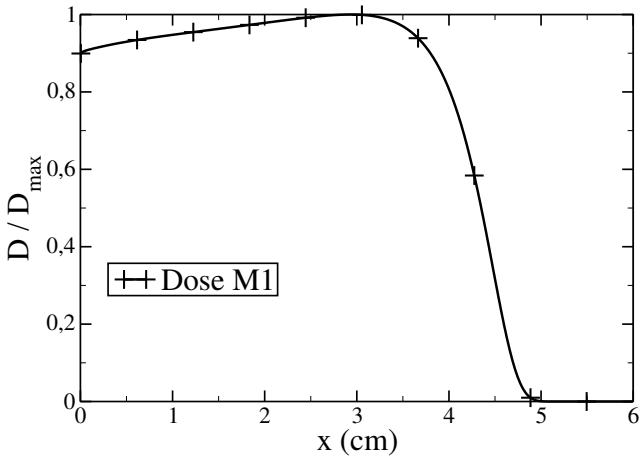

Figure 1: Normalized dose obtained with Algorithm 1 for the beam of electron (29).

better stopping criterium consists in defining the residual

$$r^{n,(k)} = \max_l \left\| -\mathbf{L}(\boldsymbol{\psi}_{l-1}^{n,(k)}) + \mathbf{D}(\boldsymbol{\psi}_l^{n,(k)}) - \mathbf{U}(\boldsymbol{\psi}_{l+1}^{n,(k)}) - \rho_l \mathbf{R}_l^n \right\|_\infty , \tag{31}$$

and chose to stop Algorithm 1 as soon as

$$r^{n,(k)} \leq r_{\max}. \tag{32}$$

The number of iterations $k_{\max}$ required to reach this criterium is ploted on Fig. 2 as a function of the energy step n, for $r_{\max}$ fixed at 10^{-1}, 10^{-2}, 10^{-3} and 10^{-4}. The final residual $r^{n,(k_{\max})}$ obtained by fixing $k_{\max}$ to 10, 30, 50 or 70 is ploted on Fig. 3 as a function of the energy step n.

During the first steps (up to $n = 8$), the value of ψ_e^b on the boundary (see (29)) is too low and the fluence ψ_e inside the medium is below the threshold δ. This explains the low values of k and of $r^{n,(k_{\max})}$ for these values of n.

In the first steps where the values of ψ_e^b is non-negligible, Algorithm 1 requires a large number of iterations to converge. At those energy, $\partial_\epsilon \boldsymbol{\psi} \equiv (\boldsymbol{\psi}^{n-1} - \boldsymbol{\psi}^n)/\Delta\epsilon^n$ is large. Thus the intialization $\boldsymbol{\psi}^{n,(0)} = \boldsymbol{\psi}^{n-1}$ of Algorithm 1 is far from the desired solution. Therefore the present algorithm requires more iterations to converge.

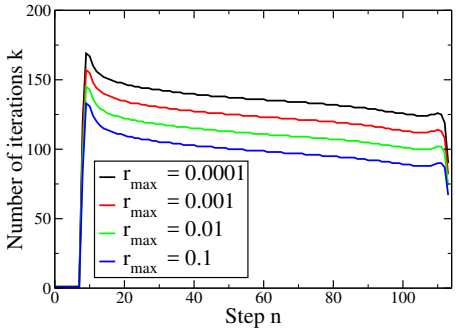

Figure 2: Number of iterations k as a function of the energy step n for a given maximum residual $r_{\max}$

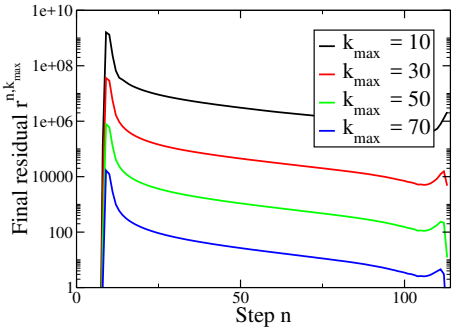

Figure 3: Final residual $r^{n,(k_{\max})}$ as a function of the energy step n for a given number of iteration $k_{\max}$

The convergence rate progressively raises, *i.e.* the final residual $r^{n,(k_{\max})}$ or the number of iterations k reduce.

The drop of $r^{n,(k_{\max})}$ and of iterations k near the end of the simulation is due to the physical parameters used. The stopping power S skyrockets near the threshold $\epsilon = \epsilon_{\min}$. According to the definition of $\mathbf{D}$ in (22), this implies that the eigenvalues of $\mathbf{D}$ also raise at such low energy. Thus the eigenvalues of J drop to zero, and so the convergence rate of Algorithm 1 skyrockets. This explains the behaviour of the curves k and $r^{n,(k_{\max})}$ in the last steps n.

In all the remaining test cases, the parameter $r_{\max}$ is fixed, and the parameter $k_{\max}$ is chosen sufficiently high such that the residual $r_{\max}$ is always reached during the computations.

3.5.2 Convergence results of the numerical scheme

In this subsection, we verify experimentally that the numerical scheme is converging. The maximum residual $r_{\max}$ was fixed at 10^{-2}.

Since no analytical solution is known, the reference solution is chosen to be the solution obtained with the largest number of cells. The spatial domain $Z = [0\text{ cm}, 6\text{ cm}]$ is uniformly meshed. The number of spatial cells $l_{\max}$ is chosen to be 300, 600, 1200, 2400 and 4800 cells and for the reference solution 9600 cells. The convergence rate in Δx is represented by the discrete L^2 error between the reference solution (*i.e.* the most refined one) and the less refined ones. This error is plotted on Fig. 4 as a function of Δx. As expected, we

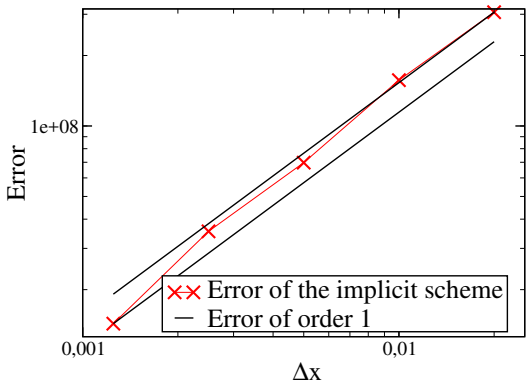

Figure 4: Discrete L^2 error compared to the most refined solution as a function of Δx with $\Delta\epsilon^n$ given by (30).

observe a convergence rate of order 1, the mean slope of the curve obtained on Fig. 4 being of 1.1046894.

4 A numerical approach for multi-D problems

We extend here the previous approach for coupled electrons and photons transport in multi-D media. The difficulties and the method are described in the next three subsection in 2D through the model

$$\partial_x \mathbf{F}_1(\boldsymbol{\psi}) + \partial_y \mathbf{F}_2(\boldsymbol{\psi}) = \rho \mathbf{Q}(\boldsymbol{\psi}). \tag{33}$$

However the method is also valid in 3D and a 3D test case is provided in Subsection 4.4.

4.1 A correction of the numerical transverse diffusion

As described in [4, 50] and through the experimental results below, using the relaxation parameters (18) when considering 2D photon beams leads to a numerical overestimation of the diffusion effects in the direction orthogonal to the beams.

In multi-D, the velocities $c^{\pm}$ are vectors instead of scalars. We consider two relaxation velocities $c_i^{\pm} = \pm|c_i^{\pm}|e_i$ per Cartesian direction e_i. The relaxation parameters need to satisfy ([43, 11, 1])

$$\forall d \in S^2, \qquad Sp\left(\mathbf{F}'_d(\boldsymbol{\psi})\right) \subset \left[\min_{i,\pm}(c_i^{\pm}.d),\ \max_{i,\pm}(c_i^{\pm}.d)\right], \tag{34a}$$

$$\sum_{i,\pm} \mathbf{M}_i^{\pm} = \boldsymbol{\psi}, \qquad \sum_{i,\pm}(c_i^{\pm}.d)\mathbf{M}_i^{\pm} = \mathbf{F}_d(\boldsymbol{\psi}), \tag{34b}$$

where

$$\mathbf{F}_d(\boldsymbol{\psi}) = d_1\mathbf{F}_1(\boldsymbol{\psi}) + d_2\mathbf{F}_2(\boldsymbol{\psi}) = (\psi_\gamma^1.d,\ \psi_\gamma^2.d,\ \psi_e^1.d,\ \psi_e^2.d)$$

is the flux in the direction d. In practice, we use the relaxation velocities $c_i^{\pm}$ defined in [50] that are assumed to approximate numerically the maximum physical velocities in each Cartesian directions

$$|c_i^{\pm}| \approx \max\left(\delta, \max\left[Sp\left(\pm\mathbf{F}'_i(\boldsymbol{\psi})\right)\right]\right),$$

where $\delta = 10^{-8}$ is a constant chosen arbitrarily small to avoid numerical divisions by zero. We use Maxwellians of the form

$$\mathbf{M}_i^{\pm} = \mu_i^{\pm}\boldsymbol{\psi} + \lambda_i^{\pm}\mathbf{F}_i(\boldsymbol{\psi}).$$

In order to satisfy (34b), one finds that $\mu_i^{\pm}$ and $\lambda_i^{\pm}$ need to satisfy

$$\sum_{i,\pm} \mu_i^{\pm} = 1, \tag{35a}$$

$$\lambda_i^- + \lambda_i^+ = 0, \qquad -|c_i^-|\mu_i^- + |c_i^+|\mu_i^+ = 0, \qquad -|c_i^-|\lambda_i^- + |c_i^+|\lambda_i^+ = 1. \tag{35b}$$

The last three equations (35b) can be rewritten

$$\mu_i^- = \frac{|c_i^+|}{|c_i^-|}\mu_i^+, \qquad \lambda_i^{\pm} = \pm\frac{1}{|c_i^+| + |c_i^-|}.$$

In practice, in 2D, we chose to fix the last degrees of freedom μ_i^+ by

$$\mu_i^{\pm} = \frac{|c_i^{\mp}|}{2(|c_i^+| + |c_i^-|)},$$

which satisfies (35a). This leads to write the Maxwellians

$$\mathbf{M}_i^{\pm} = \frac{|\tilde{c}_i^{\mp}|\boldsymbol{\psi} \pm 2\mathbf{F}_i(\boldsymbol{\psi})}{2(|\tilde{c}_i^{+}| + |\tilde{c}_i^{-}|)} \in \mathcal{R}^2, \tag{36}$$

where $|\tilde{c}_i^{\pm}|$ is either $|c_i^{\pm}|$ or the minimum scalar such that (36) is realizable.

Applying the method described in Subsection 3.2 to the 2D equation (33) leads to write the scheme

$$\frac{\mathbf{F}^n_{l+\frac{1}{2},m} - \mathbf{F}^n_{l-\frac{1}{2},m}}{\Delta x} + \frac{\mathbf{F}^n_{l,m+\frac{1}{2}} - \mathbf{F}^n_{l,m-\frac{1}{2}}}{\Delta y} - [\rho\mathbf{Q}(\boldsymbol{\psi})]^n_{l,m} = 0, \tag{37a}$$

$$\begin{aligned}\mathbf{F}^n_{l+\frac{1}{2},m} &= c^{-,n}_{l+\frac{1}{2},m}\lambda^{-,n}_{l+\frac{1}{2},m}\mathbf{F}_1(\boldsymbol{\psi}^n_{l+1,m}) + c^{+,n}_{l+\frac{1}{2},m}\lambda^{+,n}_{l+\frac{1}{2},m}\mathbf{F}_1(\boldsymbol{\psi}^n_{l,m}) \\ &\quad + \left(c^{-,n}_{l+\frac{1}{2},m}\mu^{-,n}_{l+\frac{1}{2},m}\boldsymbol{\psi}^n_{l+1,m} + c^{+,n}_{l+\frac{1}{2},m}\mu^{+,n}_{l+\frac{1}{2},m}\boldsymbol{\psi}^n_{l,m}\right), \end{aligned} \tag{37b}$$

$$\begin{aligned}\mathbf{F}^n_{l,m+\frac{1}{2}} &= c^{-,n}_{l,m+\frac{1}{2}}\lambda^{-,n}_{l,m+\frac{1}{2}}\mathbf{F}_2(\boldsymbol{\psi}^n_{l,m+1}) + c^{+,n}_{l,m+\frac{1}{2}}\lambda^{+,n}_{l,m+\frac{1}{2}}\mathbf{F}_2(\boldsymbol{\psi}^n_{l,m}) \\ &\quad + \left(c^{-,n}_{l,m+\frac{1}{2}}\mu^{-,n}_{l,m+\frac{1}{2}}\boldsymbol{\psi}^n_{l,m+1} + c^{+,n}_{l,m+\frac{1}{2}}\mu^{+,n}_{l,m+\frac{1}{2}}\boldsymbol{\psi}^n_{l,m}\right), \end{aligned} \tag{37c}$$

where the coefficients in the discrete fluxes are given by

$$\lambda^{\pm,n}_{j,k} = \pm\frac{1}{|c^{+,n}_{j,k}| + |c^{-,n}_{j,k}|}, \qquad \mu^{\pm,n}_{j,k} = \frac{|c^{\mp,n}_{j,k}|}{2(|c^{+,n}_{j,k}| + |c^{-,n}_{j,k}|)},$$

$$c^{\pm,n}_{l+\frac{1}{2},m} = \pm\max\left(|\tilde{c}_1^{\pm}(\boldsymbol{\psi}^n_{l+1,m})|, |\tilde{c}_1^{\pm}(\boldsymbol{\psi}^n_{l,m})|\right),$$

$$c^{\pm,n}_{l,m+\frac{1}{2}} = \pm\max\left(|\tilde{c}_2^{\pm}(\boldsymbol{\psi}^n_{l,m+1})|, |\tilde{c}_2^{\pm}(\boldsymbol{\psi}^n_{l,m})|\right),$$

for $(j,k) = (l+\frac{1}{2}, m)$ or $(j,k) = (l, m+\frac{1}{2})$.

4.2 An iterative solver for the multi-D scheme with the transverse diffusion correction

We propose to adapt Algorithm 1 when the coefficients $c_i^{\pm}$ are not constants. In this case, the scheme (37) can be rewritten under the form

$$\begin{aligned}\rho_l\mathbf{R}^n_l &= -\mathbf{L}_1(\boldsymbol{\psi}^n_{l-1,m}) - \mathbf{L}_2(\boldsymbol{\psi}^n_{l,m-1}) + \mathbf{D}(\boldsymbol{\psi}^n_{l,m}) \\ &\quad -\mathbf{U}_1(\boldsymbol{\psi}^n_{l+1,m}) - \mathbf{U}_2(\boldsymbol{\psi}^n_{l,m+1}),\end{aligned} \tag{38a}$$

where the operators $\mathbf{L}_1$, $\mathbf{L}_2$, $\mathbf{U}_1$, $\mathbf{U}_2$ and $\mathbf{D}$ yield

$$\mathbf{L}_1(\boldsymbol{\psi}^n_{l-1,m}) = \frac{c^{+,n}_{l-\frac{1}{2},m}}{\Delta x}\left[\mu^{+,n}_{l-\frac{1}{2},m}\boldsymbol{\psi}^n_{l-1,m} + \lambda^{+,n}_{l-\frac{1}{2},m}\mathbf{F}_1(\boldsymbol{\psi}^n_{l-1,m})\right], \tag{38b}$$

$$\mathbf{L}_2(\boldsymbol{\psi}^n_{l,m-1}) = \frac{c^{+,n}_{l,m-\frac{1}{2}}}{\Delta y}\left[\mu^{+,n}_{l,m-\frac{1}{2}}\boldsymbol{\psi}^n_{l,m-1} + \lambda^{+,n}_{l,m-\frac{1}{2}}\mathbf{F}_2(\boldsymbol{\psi}^n_{l,m-1})\right], \tag{38c}$$

$$\mathbf{U}_1(\boldsymbol{\psi}^n_{l+1,m}) = \frac{-c^{-,n}_{l+\frac{1}{2},m}}{\Delta x}\left[\mu^{-,n}_{l+\frac{1}{2},m}\boldsymbol{\psi}^n_{l+1,m} + \lambda^{-,n}_{l+\frac{1}{2},m}\mathbf{F}_1(\boldsymbol{\psi}^n_{l+1,m})\right], \tag{38d}$$

$$\mathbf{U}_2(\boldsymbol{\psi}^n_{l,m+1}) = \frac{-c^{-,n}_{l,m+\frac{1}{2}}}{\Delta y}\left[\mu^{-,n}_{l,m+\frac{1}{2}}\boldsymbol{\psi}^n_{l,m+1} + \lambda^{-,n}_{l,m+\frac{1}{2}}\mathbf{F}_2(\boldsymbol{\psi}^n_{l,m+1})\right], \tag{38e}$$

$$\mathbf{D}(\boldsymbol{\psi}^n_{l,m}) = \left(\rho_l A^n + \beta^n_{l,m} Id\right)\boldsymbol{\psi}^n_{l,m} + \gamma^n_{1,l,m}\mathbf{F}_1(\boldsymbol{\psi}^n_{l,m}) + \gamma^n_{2,l,m}\mathbf{F}_2(\boldsymbol{\psi}^n_{l,m}), \tag{38f}$$

where the coeffiecients $\beta^n_{l,m}$, $\gamma^n_{1,l,m}$ and $\gamma^n_{2,l,m}$ read

$$\beta^n_{l,m} = \frac{c^{+,n}_{l+\frac{1}{2},m}\mu^{+,n}_{l+\frac{1}{2},m} - c^{-,n}_{l-\frac{1}{2},m}\mu^{-,n}_{l-\frac{1}{2},m}}{\Delta x} + \frac{c^{+,n}_{l,m+\frac{1}{2}}\mu^{+,n}_{l,m+\frac{1}{2}} - c^{-,n}_{l,m-\frac{1}{2}}\mu^{-,n}_{l,m-\frac{1}{2}}}{\Delta y},$$

$$\gamma^n_{1,l,m} = \frac{c^{+,n}_{l+\frac{1}{2},m}\lambda^{+,n}_{l+\frac{1}{2},m} - c^{-,n}_{l-\frac{1}{2},m}\lambda^{-,n}_{l-\frac{1}{2},m}}{\Delta x},$$

$$\gamma^n_{2,l,m} = \frac{c^{+,n}_{l,m+\frac{1}{2}}\lambda^{+,n}_{l,m+\frac{1}{2}} - c^{-,n}_{l,m-\frac{1}{2}}\lambda^{-,n}_{l,m-\frac{1}{2}}}{\Delta y}.$$

The difficulty here emerges from the non-linearity of the operator $\mathbf{D}$ to invert and from the realizability requirements (34).

Let us decompose the operator $\mathbf{D}$ into

$$\begin{aligned}\mathbf{D}(\boldsymbol{\psi}) &= \mathbf{D}_{imp}(\boldsymbol{\psi}) - \mathbf{D}_{exp}(\boldsymbol{\psi}),\\ \mathbf{D}_{imp}(\boldsymbol{\psi}) &= \left[\rho_l A^n + (\alpha^n_{l,m} + \beta^n_{l,m})Id\right]\boldsymbol{\psi},\\ \mathbf{D}_{exp}(\boldsymbol{\psi}) &= \alpha^n_{l,m}\boldsymbol{\psi} + \gamma^n_{1,l,m}\mathbf{F}_1(\boldsymbol{\psi}) + \gamma^n_{2,l,m}\mathbf{F}_2(\boldsymbol{\psi}),\end{aligned} \tag{39}$$

such that $\mathbf{D}_{imp}$ is linear and invertible. Here the coefficient $\alpha^n_{l,m}$ is chosen non-negative such that the operator $\mathbf{D}_{exp}$ preserves the realizability. In practice, one may simply chose

$$\alpha^n_{l,m} = |\gamma^n_{1,l,m}| + |\gamma^n_{2,l,m}|.$$

Finally, Algorithm 1 is rewritten by modifying (23). This leads to the following algorithm.

Algorithm 2. *Initialization:* Set $\boldsymbol{\psi}_{l,m}^{n,(0)} = \boldsymbol{\psi}_{l,m}^{n-1}$ for all l, m.
Iteration: Compute iteratively

$$\begin{aligned}\boldsymbol{\psi}_{l,m}^{n+1,(k+1)} &= \mathbf{D}_{imp}^{-1}\Big(\mathbf{R}_{l,m}^{n} + \mathbf{L}_1(\boldsymbol{\psi}_{l-1,m}^{n+1,(k)}) + \mathbf{L}_2(\boldsymbol{\psi}_{l,m-1}^{n+1,(k)}) \\ &\quad + \mathbf{D}_{exp}(\boldsymbol{\psi}_{l,m}^{n+1,(k)}) + \mathbf{R}_1(\boldsymbol{\psi}_{l-1,m}^{n+1,(k)}) + \mathbf{R}_2(\boldsymbol{\psi}_{l,m-1}^{n+1,(k)})\Big),\end{aligned} \tag{40}$$

until convergence.

Remark 6.

- The parameter $\alpha^n Id$ was artificially added on both sides of (39) when splitting the operator $\mathbf{D}$ in two parts. This enforces the preservation of the realizability property and makes the algorithm more stable. However, this reduces the convergence rate of Algorithm 2.
- One may reproduce the computations from the proof of Proposition 1 with (40) to show that the realizability property is preserved from one iteration to another in Algorithm 2 and to show it is convergent.

4.3 Numerical experiment in 2D: a photon beam in water

In this test case, photons are injected in a 2D homogeneous domain composed of water. The size of the medium is 2 cm × 10 cm, and a 0.5 cm large beam of 500 keV photons is injected on the left boundary. This is modeled by the following incoming boundary condition

$$\begin{aligned}\text{for} \quad (X,\Omega) \in \Gamma^- &= \left\{(X,\Omega) \in \partial Z \times S^2 \quad \text{s.t.} \quad n(x).\Omega < 0\right\}, \\ \psi_\gamma(X,\epsilon,\Omega) &= 10^{10}\exp\left(-\alpha_\epsilon\left(\epsilon-\epsilon_0\right)^2\right)\exp\left(-\alpha_\mu\left(\Omega_1-1\right)^2\right)\mathbf{1}_B(X) \\ &\quad + \delta\mathbf{1}_{\partial Z\setminus B}(X), \\ \psi_e(X,\epsilon,\Omega) &= \delta, \\ B &= \left\{(x,y), \quad x=0, \quad y\in[0.75\text{ cm}, 1.25\text{ cm}]\right\},\end{aligned}$$

where $n(x)$ is the outgoing normal, $\epsilon_0 = 500$ keV, $\alpha_\epsilon = 20000$, $\alpha_\mu = 500000$ and $\delta = 10^{-15}$. And we used the moments of those distribution as boundary conditions for the moment equations.

Through this test case, we aim to highlight the influence of the choice of the parameters $c^\pm$ on the convergence rate of Algorithm 1. The influence of $c^\pm$ on the dose results were studied in [50] and are only recalled here for completeness. The present method is tested using two sets of parameters $c_i^\pm$:

- First, we fix $|c_i^{\pm}| = 2$ at a sufficiently large value (afterward called large c) for the conditions (34) to be satisfied. Those parameters were shown to provide an overestimated numerical angular diffusion in [50] (see also Fig. 5 below).

- Second, we fix $c_i^{\pm}$ at a value closer to the value actual eigenvalues of the Jacobian of the flux as proposed in [50] (afterward called small c). These parameters were shown to reduce the diffusion effects of the numerical method, especially in the direction orthogonal to the beam.

Algorithm 2 is compared to a reference Monte Carlo solver ([23]). The dose results obtained with those methods are gathered on Fig. 5 with the computational times in Table 1. A cut of the doses along the axis of the beam $y = 1$ cm and in the transverse direction at depth $x = 2$ cm and $x = 8$ cm are shown on Fig. 6.

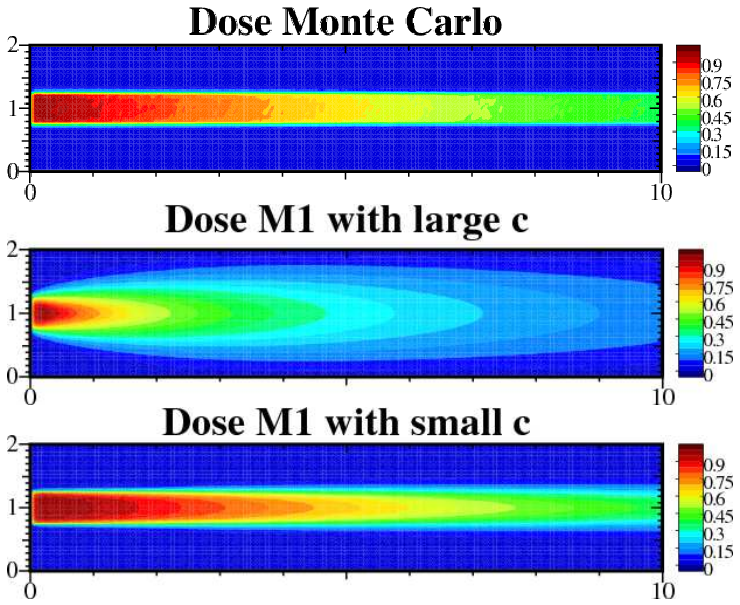

Figure 5: Doses obtained with the Monte Carlo solver (top) and the M_1 solver with large c (middle) and small c (below) relaxation parameters, normalized by their maximum value.

Solver	Monte Carlo	M_1 with large c	M_1 with small c
Computation times	14 hours	49.78699 sec	204.1239 sec

Table 1: Computational times with the Monte Carlo solver and the implicit solver with the different c.

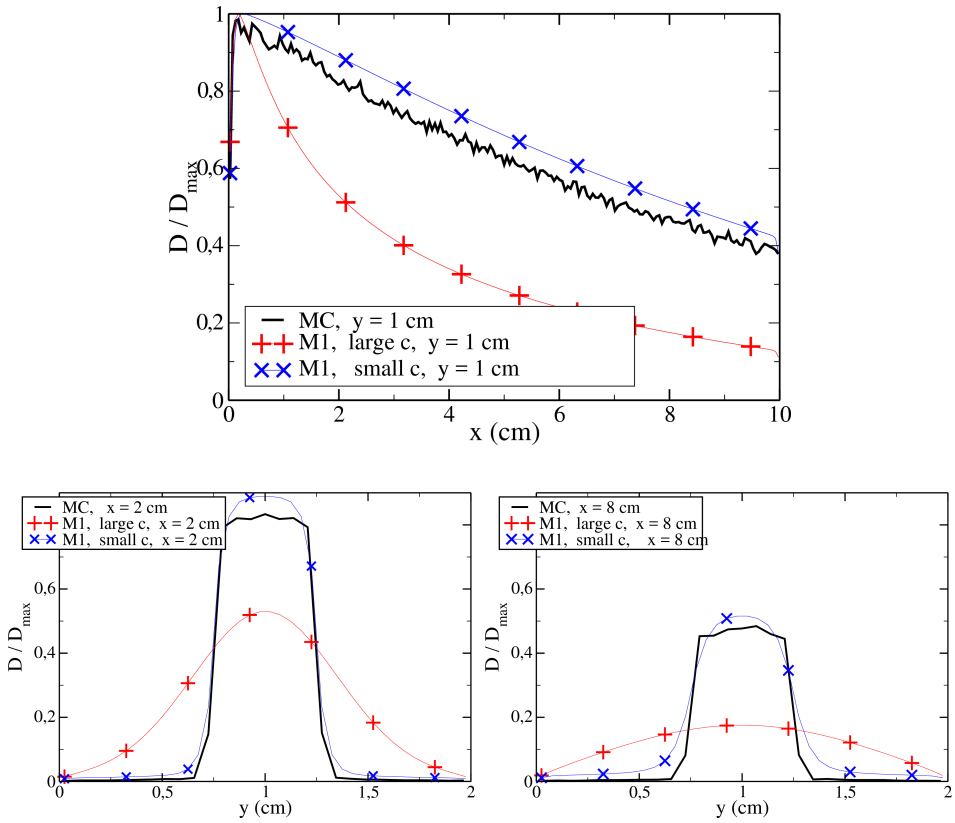

Figure 6: Doses obtained with the Monte Carlo solver and the M_1 solver with large and small c along the axis of the beam (top) and the axis transverse to the beam at 2 cm depth (below left) and 8 cm depth (below right), normalized by their maximum value.

The dose results with the modified relaxation parameters are much closer to the reference Monte Carlo results. As expected the dose is less diffused with the small c.

Due to the noise in the Monte Carlo and the normalization by $\max D$, the M_1 dose curves with the modified relaxation parameters are slightly above the Monte Carlo reference on Fig. 6.

Following Remark 6, we observe that the computational time is higher with the small c than with the large ones. Those times remains much lower than the one with the Monte Carlo reference.

4.4 Numerical experiment in 3D: a photon beam in a chest

This test case aims to exhibit the efficiency of our method when considering more complex density maps. For this purpose, a density map obtained from a computed tomography (CT) scan of a chest is used. This map is depicted on Fig. 7. This domain is a 29.5 cm deep cube.

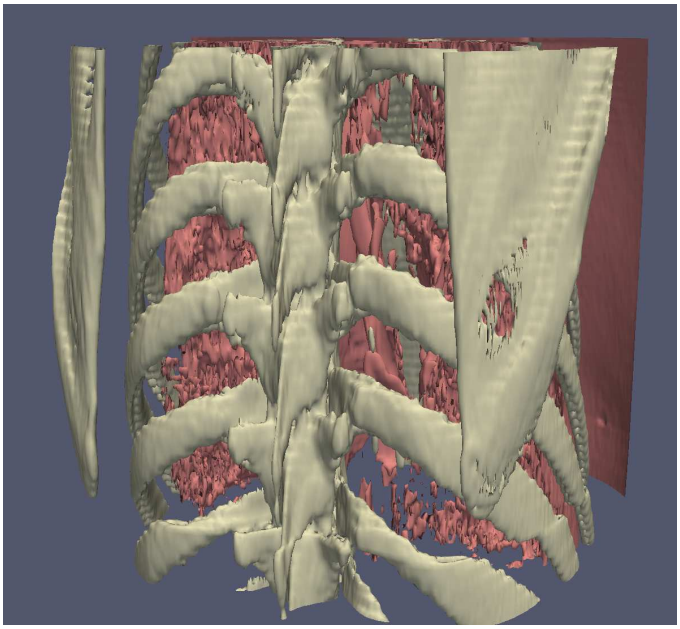

Figure 7: Density map represented by isosurfaces of density 1.8 (ivory; equivals to bone density) and 0.3 (flesh colour; equivals to lung density).

A beam of photons is imposed on the boundary of the medium to pass through the ribs. In order to reduce the computational time, the computa-

tions are performed on a smaller domain of size 14 cm $\times$ 25 cm $\times$ 11.35 cm in which the density of photons is non-negligible. This domain is meshed with $140 \times 220 \times 50$ cells.

The beam is modeled by the following condition over Γ^-

$$\begin{aligned}
\psi_\gamma(X,\epsilon,\Omega) &= 10^{10}\exp\left(-\alpha_\epsilon\left(\epsilon-\epsilon_0\right)^2\right)\exp\left(-\alpha_\mu\left(\Omega_2-1\right)^2\right)\mathbf{1}_B(X) \\
&\quad +\delta\mathbf{1}_{\partial Z\setminus B}, \\
\psi_e(X,\epsilon,\Omega) &= \delta,
\end{aligned}$$

$$B=\left\{(x,y,z),\quad x\in[6\text{ cm},8\text{ cm}],\ y=0\text{ cm},\ z\in[4\text{ cm},6\text{ cm}]\right\},$$

where $n(x)$ is the outgoing normal, $\epsilon_0 = 1$ MeV, $\alpha_\epsilon = 20000$, $\alpha_\mu = 3000$ and $\delta = 10^{-15}$. And we used the moments of those distribution as boundary conditions for the moment equations.

The maximum residual was fixed at $r_{\max} = 10^{-1}$.

The computations were performed with the small parameters c. Those dose results are depicted on Fig. 8 as isodose surfaces cut along the surfaces parametrized by $\{x = 5\text{ cm}\}$, $\{y = 12.5\text{ cm}\}$ and $\{z = 5.675\text{ cm}\}$, that are along the axis of the beam or at half depth in the domain.

The present method was tested on a rather complex problem with a large 3D mesh, a complete physics (photons and electrons together) and using the large c, that is in the most complex settings. The computations were performed in parallel on four cores and the computational times are gathered in Table 2. These times of computataion remains too long for practical

Solver	M_1 with small c
Computation times	10405 sec $\approx$ 2 h 53 min

Table 2: Computational times with the implicit solver for the 3D problem.

applications in medical physics. Several features in our approach can be improved to reduce drastically the computational times. The main time consuming issue and an axe of improvement are presented here.

In practice, the moments $\boldsymbol{\psi}$ are computed in the whole space-energy domain, even in cells where they are negligible. This results in solving (40) over a very large vector $\boldsymbol{\psi}^n$. Those non-necessary computations raise the size of the system to solve and reduce the convergence rate of our algorithm (see Remark 5).

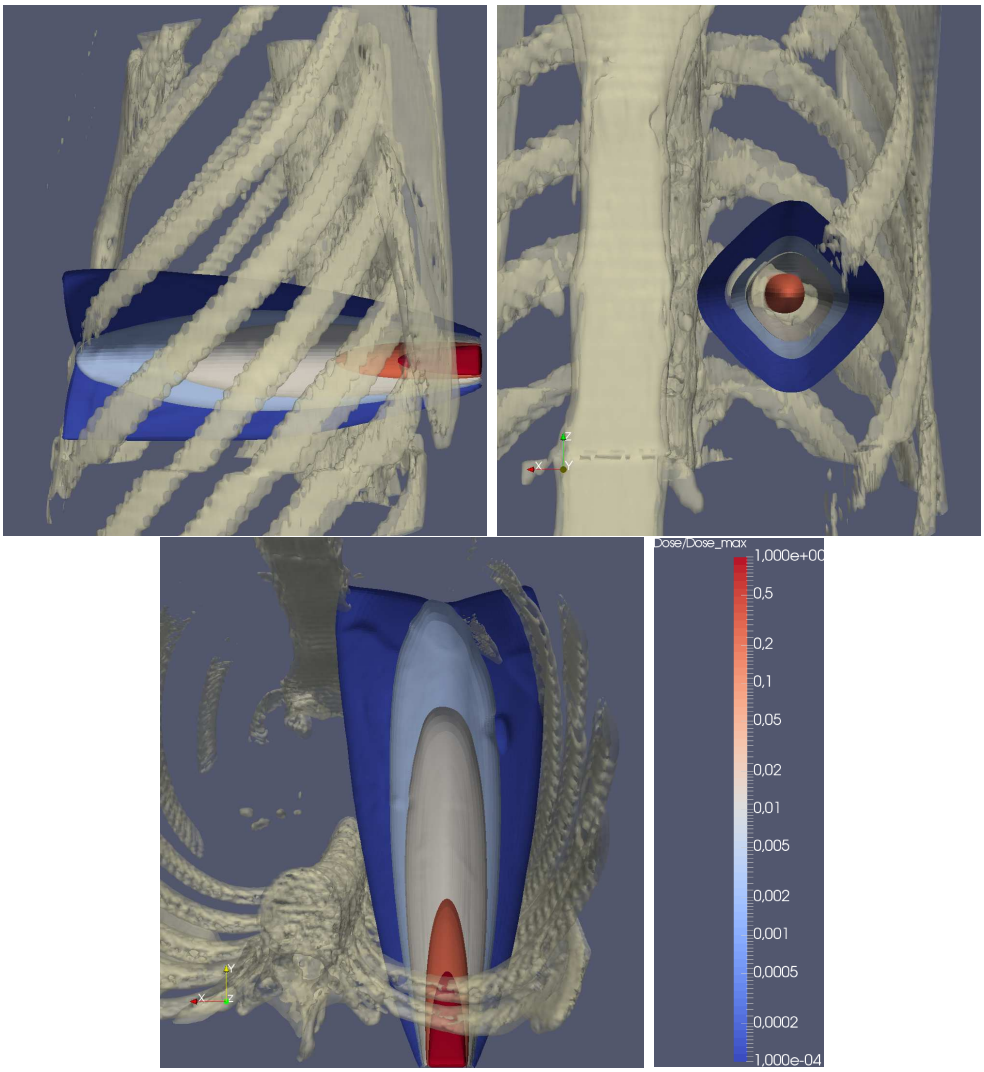

Figure 8: Isosurfaces of dose at 60%, 30%, 6%, 3% and 0.6% of the maximum dose in a chest.

The computational times can be considerably reduced using common code optimization techniques. The most common idea for such a problem is the mesh adaptation, here over the space and the energy. Instead of computing $\boldsymbol{\psi}$ in the whole domain, one may solve (40) on a smaller domain where $\boldsymbol{\psi}$ is expected not to be negligible. This would lead to a considerable reduction of

both the computational times and the memory requirements. This method was also used in the development of the industrial code Acuros® [24] with considerable ressources requirement reduction.

5 Conclusions

The present approach aims to circumvent restrictive stability conditions when numerically solving coupled linear kinetic equations.

First, an angular moment extraction was performed leading to a so-called M_1 system of equations. Such models require lower computational cost to solve, but are valid under a realizability condition.

A numerical scheme for M_1 systems was proposed by chosing implicit flux and collision terms. Then an iterative method was constructed to compute the solution of such an implicit scheme. The proposed algorithm was constructed with a special focus on the preservation of the realizability property.

Numerical experiments showed that our method behaves appropriately in practical cases in 1D and in multi-D and the convegence of the method was tested in 1D. The present approach was shown to require much lower computational costs than a reference Monte Carlo method.

Acknowledgement

The authors are grateful to Gabriele Birindelli (Université de Bordeaux) and Kerstin Küpper (RWTH Aachen) for performing the PENELOPE simulations, and to Martin Frank (RWTH Aachen) for fruitful discussions. This work was partially funded by Aquitaine Region and FEDER fund through IOPRA interface. T. Pichards PhD and postdoctoral research were funded respectively by IdEx Bordeaux and Aquitaine Region; and by CEA and LJLL through LRC Manon.

References

[1] D. Aregba-Driollet and R. Natalini. Discrete kinetic schemes for multidimensional systems of conservation laws. *SIAM J. Numer. Anal.*, 6:1973–2004, 2000.

[2] D. Aregba-Driollet, R. Natalini, and S. Tang. Explicit diffusive kinetic schemes for nonlinear degenerate parabolic systems. *Math. Comp.*, 73:63–94, 2004.

[3] O. Axelsson. *Iterative solution methods*. Cambridge University Press, New York, NY, USA, 1994.

[4] C. Berthon, P. Charrier, and B. Dubroca. An HLLC scheme to solve the M_1 model of radiative transfer in two space dimensions. *J. Sci. Comput.*, 31(3):347–389, 2007.

[5] C. Berthon, M. Frank, C. Sarazin, and R. Turpault. Numerical methods for balance laws with space dependent flux: Application to radiotherapy dose calculation. *Commun. Comput. Phys.*, 10(5), 2011.

[6] G. Birindelli, J.-L. Feugeas, J. Caron, B. Dubroca, G. Kantor, J. Page, T. Pichard, V. T. Tikhonchuk, and Ph. Nicolaï. High performance modelling of the transport of energetic particles for photon radiotherapy. *Phys. Med., spec. issue SFPM 2016 conference*, to appear.

[7] R. Borsche, J. Kall, A. Klar, and T.N.H. Pham. Kinetic and related macroscopic models for chemotaxis on networks. *Math. Mod. Meth. Appl. S.*, 26(6):1219–1242, 2016.

[8] J. Borwein and A. Lewis. Duality relationships for entropy-like minimization problems. *SIAM J. Control Optim.*, 29(2):325–338, 1991.

[9] J. Borwein and A. Lewis. Partially finite convex programming, part I: Quasi relative interiors and duality theory. *Math. Program.*, 57:15–48, 1992.

[10] J. Borwein and A. Lewis. Partially finite convex programming: Part II. *Math. Program.*, 57:49–83, 1992.

[11] F. Bouchut. Construction of BGK models with a family of kinetic entropies for a given system of conservation laws. *J. Stat. Phys.*, 95(1):113–170, 1998.

[12] F. Bouchut, F. R. Guarguaglini, and R. Natalini. Diffusive bgk approximations for nonlinear multidimensional parabolic equations. *Indiana Univ. Math. J.*, 49:723–749, 2000.

[13] T. A. Brunner and J. P. Holloway. One-dimensional riemann solvers and the maximum entropy closure. *J. Quant. Spectros. Radiat. Transfer*, 69(5):543 – 566, 2001.

[14] J. Caron, J.-L. Feugeas, B. Dubroca, G. Kantor, C. Dejean, G. Birindelli, T. Pichard, Ph. Nicolaï, E. d'Humières, M. Frank, and V. Tikhonchuk. Deterministic model for the transport of energetic particles: Application in the electron radiotherapy. *Phys. Medica*, 31(8):912–921, 2015.

[15] CERN. *Geant4 user's guide for application developers*, 2015.

[16] S. Chandrasekhar. On the radiative equilibrium of a stellar atmosphere. *Astrophys. J.*, 99:180 – 190, 1943.

[17] S. Chandrasekhar. On the radiative equilibrium of a stellar atmosphere X. *Astrophys. J.*, 103:351 – 370, 1946.

[18] D. Coulette, E. Franck, P. Helluy, M. Mehrenberger, and L. Navoret. Palindromic discontinuous Galerkin method for kinetic equations with stiff relaxation. *Hal archives ouvertes*, 2016.

[19] B. Dubroca and J.-L. Feugeas. Hiérarchie des modèles aux moments pour le transfert radiatif. *C. R. Acad. Sci. Paris*, 329:915–920, 1999.

[20] B. Dubroca and M. Frank. An iterative method for transport equations in radiotherapy. *Progress in Industrial Mathematics at ECMI 2008*, pages 407–412, 2010.

[21] R. Duclous, B. Dubroca, and M. Frank. A deterministic partial differential equation model for dose calculation in electron radiotherapy. *Phys. Med. Biol.*, 55:3843–3857, 2010.

[22] L. Elsner and V. Mehrmann. Convergence of block iterative methods for linear systems arising in the numerical solution of euler equations. *Numer. Math.*, 59(1):541–559, 1991.

[23] J. Sempau F. Salvat, J. M. Fernández-Varea. *PENELOPE-2011: A code system for Monte Carlo simulation of electron and photon transport*, 2011.

[24] G.A. Failla, T.A. Wareing, Y. Archambault, and S. Thompson. Acuros XB ® advanced dose calculation for the Eclipse ™ treatement planning system. *Clinical perspectives*, 2010.

[25] B. D. Ganapol, C. T. Kelley, and G. C. Pomraning. Asymptotically exact boundary conditions for the P_N equations. *Nucl. Sci. Eng.*, 114, 1993.

[26] C. Groth and J. McDonald. Towards physically realizable and hyperbolic moment closures for kinetic theory. *Cont. Mech. Therm.*, 21(6):467–493, 2009.

[27] T. Hanawa and E. Audit. Reformulation of the M_1 model of radiative transfer. *J. Quant. Spectros. Radiat. Transfer*, 145:9 – 16, 2014.

[28] A. Harten, P. Lax, and B. Van Leer. On upstream differencing and Gudonov-type schemes for hyperbolic conservation laws. *SIAM Rev.*, 25(1):35–61, 1983.

[29] C. Hauck. *Entropy-based moment closures in semiconductor models*. PhD thesis, University of Maryland, 2006.

[30] C. D. Hauck, C. D. Levermore, and A. L. Tits. Convex duality and entropy-based moment closures: Characterizing degenerate densities. *SIAM J. Control Optim.*, 2007.

[31] M. Junk. Maximum entropy for reduced moment problems. *Math. Mod. Meth. Appl. S.*, 10(1001–1028):2000, 1998.

[32] I. Kawrakow and D. W. Rogers. *The EGSnrc code system*, 2013.

[33] C. Kelley. *Iterative methods for linear and nonlinear equations*. SIAM, 1995.

[34] D. Kershaw. Flux limiting nature's own way. Technical report, Lawrence Livermore Laboratory, 1976.

[35] Los Alamos National Laboratory. *MCNP - A general Monte Carlo N-particle transport code, Version 5*, 2003.

[36] E. W. Larsen and G. C. Pomraning. The P_N theory as an asymptotic limit of transport theory in planar geometry I: Analysis. *Nucl. Sci. Eng.*, 109(49), 1991.

[37] T. Leroy, R. Duclous, B. Dubroca, V.T. Tikhonchuk, S. Brull, A. Decoster, M. Lobet, and L. Gremillet. Deterministic and stochastic kinetic descriptions of electron-ion Bremsstrahlung: From thermal to non-thermal regimes, 2014. Project at CEMRACS.

[38] C. D. Levermore. Moment closure hierarchies for kinetic theories. *J. Stat. Phys.*, 83(5–6):1021–1065, 1996.

[39] E. E. Lewis and W. F. Miller. *Computational methods of neutron transport*. American nuclear society, 1993.

[40] P. Mayles, A. Nahum, and J.C. Rosenwald, editors. *Handbook of radiotherapy physics: Theory and practice*. Taylor & Francis, 2007.

[41] J. Mcdonald and M. Torrilhon. Affordable robust moment closures for CFD based on the maximum-entropy hierarchy. *J. Comput. Phys.*, 251:500–523, 2013.

[42] G. N. Minerbo. Maximum entropy Eddington factors. *J. Quant. Spectros. Radiat. Transfer*, 20:541–545, 1978.

[43] R. Natalini. A discrete kinetic approximation of entropy solutions to multidimensional scalar conservation laws. *J. Differ. Equations*, 148(2):292 – 317, 1998.

[44] E. Olbrant and M. Frank. Generalized Fokker-Planck theory for electron and photon transport in biological tissues: Application to radiotherapy. *Comput. Math. Methods Med.*, 11(4):313–339, 2010.

[45] J. Page, J.-L. Feugeas, G. Birindelli, J. Caron, B. Dubroca, G. Kantor, T. Pichard, V.T. Tikhonchuk, and Ph. Nicolaï. New fast entropic algorithm for MRI-guided radiotherapy. *Phys. Med., spec. issue SFPM 2016 conference*, to appear.

[46] T. Pichard. *Mathematical modelling for dose deposition in photontherapy*. PhD thesis, Université de Bordeaux and RWTH Aachen University, 2016.

[47] T. Pichard, G.W. Alldredge, S. Brull, B. Dubroca, and M. Frank. The M_2 model for dose simulation in radiation therapy. *J. Comput. Theor. Transport, spec. issue ICTT 2015 conference*, 2016.

[48] T. Pichard, G.W. Alldredge, S. Brull, B. Dubroca, and M. Frank. An approximation of the M_2 closure: Application to radiotherapy dose simulation. *J. Sci. Comput*, 71(1):71–108, 2017.

[49] T. Pichard, D. Aregba-Driollet, S. Brull, B. Dubroca, and M. Frank. Relaxation schemes for the M_1 model with space-dependent flux: Application to radiotherapy dose calculation. *Commun. Comput. Phys.*, 19:168–191, 2016.

[50] T. Pichard, S. Brull, B. Dubroca, and M. Frank. On the transverse diffusion of beams of photons in radiation therapy. *Proc. HYP2016 conference*, to appear.

[51] G. C. Pomraning. *The equations of radiation hydrodynamics*. Pergamon Press, 1973.

[52] S. La Rosa, G. Mascali, and V. Romano. Exact maximum entropy closure of the hydrodynamical model for Si semiconductors: The 8-moment case. *SIAM J. Appl. Math.*, 70(3):710–734, 2009.

[53] R. P. Rulko, E. W. Larsen, and G. C. Pomraning. The P_N theory as an asymptotic limit of transport theory in planar geometry II: Numerical results. *Nucl. Sci. Eng.*, 109(76), 1991.

[54] J. Schneider. Entropic approximation in kinetic theory. *ESAIM-Math. Model. Num.*, 38(3):541–561, 2004.

[55] A. van der Sluis. Gershgorin domains for partitioned matrices. *Linear Algebra Appl.*, 26:265 – 280, 1979.

[56] M.N. Vrahatis, G.D. Magoulas, and V.P. Plagianakos. From linear to nonlinear iterative methods. *Appl. Numer. Math.*, 45(1):59 – 77, 2003.